Elastic characterization of closed cell foams from impedance tube absorption tests

F. Chevillotte and R. Panneton[a)]

GAUS, Department of Mechanical Engineering, Université de Sherbrooke, Sherbrooke Quebec, Canada, J1K2R1

A method is presented to determine the bulk elastic properties of isotropic elastic closed-cell foams from impedance tube sound absorption tests. For such foams, a resonant sound absorption is generally observed, where acoustic energy is transformed into mechanical vibration, which in turn is dissipated into heat due to structural damping. This article shows how the bulk Young's modulus, Poisson's ratio, and damping loss factor can be deduced from the resonant absorption. Also, an optimal damping loss factor yielding 100% of absorption at the first resonance is defined from the developed theory. The method is introduced for a sliding edge condition which is an ideal condition. Then, the method is extended to a bonded edge condition which is more easily achievable and additionally enables the identification of the Poisson's ratio. The method is experimentally tested on expanding closed-cell foams to find their elastic properties in both cases. Using the found properties, sound absorption predictions using an equivalent solid model with and without surface absorption are compared to measurements. Good correlations are obtained when considering surface absorption. © *2007 Acoustical Society of America.* [DOI: 10.1121/1.2783126]

I. INTRODUCTION

Many authors worked on the propagation of acoustical and elastic waves in elastic open-cell porous materials. The most used model is the one proposed by Biot[1] in which the porous medium is modelled in two superimposed phases (fluid and solid). The fluid phase (usually air) forms an interconnected cell network which opens to the surrounding medium. The two phases are elastically coupled and a relative motion between the two phases exists. Three waves propagate in the porous material (two compressional waves and one shear wave). The energy carried by the waves is dissipated through structural damping loss, viscous loss (due to relative motion between the two phases), and thermal loss.[2] In the case of elastic closed-cell foams, there is no relative motion between the fluid and solid phases. Consequently, the only energy dissipation mechanisms are the structural damping and thermal losses.[3] From the Biot's theory, only the elastic compression and shear waves now propagate in the closed-cell foams. In this case, few specific models were proposed to study the acoustic dissipation within this type of foams. The most common way of modelling these foams is to use a solid model with equivalent elastic properties. Ingard[3] proposed a method to derive these equivalent properties from the knowledge of the elastic properties of the material from which the skeleton is made, and the properties of the trapped air in the closed cells. The equivalent properties independently account for the thermal loss (which is frequency dependent) and the structural damping loss of the skeleton material. However, in many situations the properties of the skeleton material are not known

after the foaming process. Also, even if the core of these foams is made of closed cells (i.e., no propagation of acoustical waves within the core), their surface may show some irregularities and open cells (e.g., exploded cells). In this case, the surface may be seen as a thin resistive layer showing some surface sound absorption.

To account for the surface sound absorption of closed-cell foams, a model was worked out by Wojtowicki and Panneton.[4] In this work, it was shown that closed cell foams show resonant sound absorption (i.e., sound absorption at elastic resonances) with residual surface absorption (apart from resonances). To model this type of acoustic behavior, the closed-cell foams are modeled as a two-layer material: A resistive layer covering a core made of an equivalent solid with bulk elastic properties. The bulk elastic properties account for the structural damping and thermal losses. The resistive surface layer is characterized by its static airflow resistivity. Although the resistivity can be easily identified, the key element in the proper use of this so-called "surface absorption solid model" is the fine characterization of the bulk elastic properties.

The main objective of this work is to develop a method, based on sound absorption measurements, for the characterization of the bulk elastic properties of closed-cell foams—notably those from heat expanding foam process.[4] In this particular case, the produced samples have generally irregular surface and thickness that prevent the use of existing methods for the elastic characterization of column foam samples.[5–10] Brief descriptions of these methods are given elsewhere.[5]

This article is organized as follows. In Sec. II, the theory behind the method is first introduced for the sliding edge condition for which the Young's modulus and damping loss factor can be deduced. Then, the method is extended to the

---
[a)]Author to whom correspondence should be addressed. Electronic mail: raymond.panneton@usherbrooke.ca
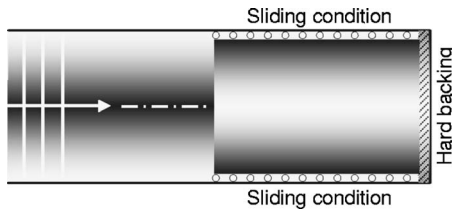
FIG. 1. Configuration of the equivalent solid foam column tested in a rigid wall impedance tube.

bonded edge condition which additionally allows for the identification of the Poisson's ratio. In Sec. III, the method is experimentally tested for characterizing the bulk elastic properties of two foams: one with the sliding edge condition and one with the bonded edge condition. Then, sound absorption predictions using the identified bulk elastic properties are compared to impedance tube results. Finally, Sec. IV concludes this work.

II. THEORY

A. Sliding edge condition

1. First natural frequency

In the following, the elastic closed-cell foam under consideration is considered as being isotropic and homogeneous so it can be modeled *a priori* as an equivalent solid. Also, it is assumed that its elastic properties are constant, or only slightly vary, with the frequency—at least around the first resonant absorption frequency. A column of this foam is now excited by a normal incidence acoustic plane wave as shown in Fig. 1. The column is backed by a rigid wall and a sliding condition is applied on its periphery. Although it is difficult to obtain in practice, the sliding condition may be approximated by lubricating the sample periphery and slightly undercutting sample diameter. Under this configuration, the normal sound absorption is of a resonant type[3,4] with the first peak absorption occurring at the first compression natural frequency of the column[11]

$$f_1 = \frac{\omega_1}{2\pi} = \frac{1}{4L}\sqrt{\frac{K_b}{\rho_1}}, \qquad (1)$$

where L is the height of the column, ρ_1 the bulk density of the foam, and K_b its bulk compression modulus.

2. Finding Young's modulus

Assuming that the height and the bulk density are known, the first resonant frequency is determined from the normal sound absorption coefficient curve and the bulk modulus of the foam is deduced from Eq. (1):

$$K_b = \rho_1(4f_1L)^2. \qquad (2)$$

As the equivalent solid is isotropic, one can relate the bulk modulus to the Young's modulus E and Poisson's ratio ν by

$$K_b = E\frac{(1-\nu)}{(1+\nu)(1-2\nu)}. \qquad (3)$$

Equation (3) shows that an infinite number of couples (E, ν) yields the same bulk modulus K_b. Hence, the Poisson's ratio

is required in order to find the Young's modulus from the bulk modulus. Assuming Poisson's ratio known, the Young's modulus is given by

$$E = \frac{(1+\nu)(1-2\nu)}{(1-\nu)}K_b. \qquad (4)$$

As the Poisson's ratio has little influence for a sliding edge condition, and based on the works by Gibson *et al.*,[12] a mean Poisson's ratio of 0.33 can be used for typical closed-cell foams. Also, as Poisson's ratio is only slightly frequency dependent, one could use a static method to measure the Poisson's ratio.

3. Finding bulk damping loss factor

The normal sound absorption coefficient of the column shown in Fig. 1 is expressed in terms of its surface acoustic impedance Z_s and the characteristic impedance of air Z_0

$$\alpha(\omega) = 1 - \left|\frac{Z_s(\omega) - Z_0}{Z_s(\omega) + Z_0}\right|^2, \qquad (5)$$

where ω is the angular frequency. As the cells of the foam are closed, there is no relative motion between the air in the cells and the structure, therefore no friction losses as in open-cell foams.[3] The only losses are due to structural damping and heat conduction (relative to the harmonic compression of the air in the cells). Making use of a bulk damping loss factor η combining both dissipation mechanisms, the losses can now be introduced in the bulk modulus as follows:

$$\widetilde{K}_b = K_b\sqrt{1 + j\eta}. \qquad (6)$$

Considering only elastic compressional waves in the material, the normal surface impedance of the sliding edge sample on hard backing may be written as

$$Z_s = \sqrt{\rho_1\widetilde{K}_b}\coth\left(j\omega L\sqrt{\frac{\rho_1}{\widetilde{K}_b}}\right), \qquad (7)$$

where $(\rho_1\widetilde{K}_b)^{1/2}$ is the characteristic impedance of the material, and $(\rho_1/\widetilde{K}_b)^{1/2}$ is the inverse of the propagation speed of the compressional waves in the material. Using Eqs. (1) and (6), the surface impedance (7) now rewrites

$$Z_s = \frac{2}{\pi}\rho_1\omega_1 L\sqrt{1 + j\eta}\coth\left(j\frac{\pi}{2}\frac{\omega}{\omega_1}\frac{1}{\sqrt{1 + j\eta}}\right). \qquad (8)$$

At the first resonance ($\omega = \omega_1$), the surface impedance becomes

$$Z_s(\omega_1) = \rho_1\omega_1 L\left(\coth\left(j\frac{\pi}{2}\frac{1}{\sqrt{1 + j\eta}}\right)\middle/\frac{\pi}{2}\frac{1}{\sqrt{1 + j\eta}}\right). \qquad (9)$$

Assuming the damping loss factor is low enough (less than 1), Eq. (9) simplifies to

$$Z_s(\omega_1) \cong \tfrac{1}{2}\rho_1\omega_1 L\eta. \qquad (10)$$

Consequently, at the first elastic resonance, substituting Eq. (10) into Eq. (5) yields the approximated sound absorption coefficient
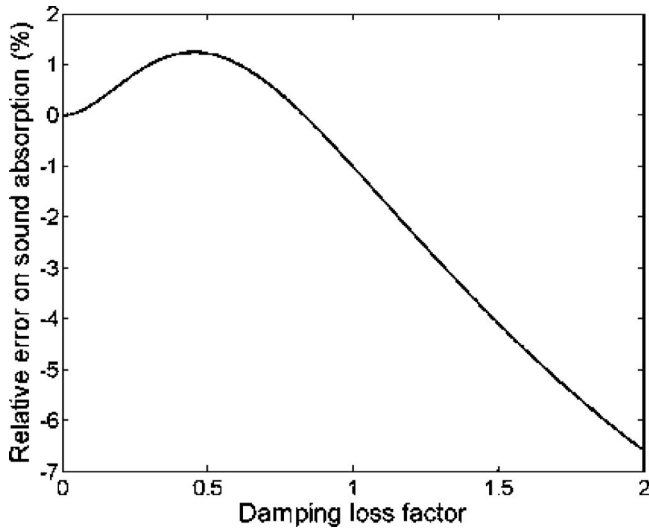
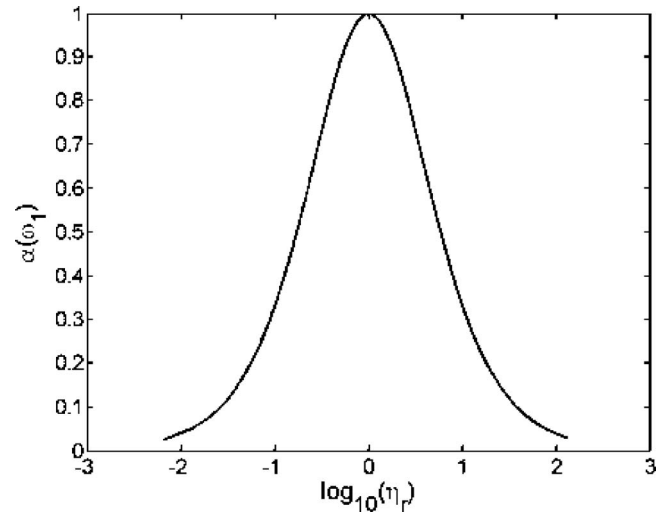FIG. 2. Relative error on sound absorption due to the approximated surface impedance [Eq. (10)].

FIG. 3. Sound absorption coefficient at the first resonance in function of the reduced structural damping loss factor for closed-cell foams.

$$\alpha(\omega_1) = 1 - \left| \frac{\rho_1 \omega_1 L \eta - 2Z_0}{\rho_1 \omega_1 L \eta + 2Z_0} \right|^2, \tag{11}$$

or, using Eq. (1),

$$\alpha(\omega_1) = 1 - \left| \frac{\pi \sqrt{\rho_1 K_b} \eta - 4Z_0}{\pi \sqrt{\rho_1 K_b} \eta + 4Z_0} \right|^2. \tag{12}$$

Equation (11) implies that the bulk damping loss factor of the material can be deduced from the sound absorption coefficient, knowing the bulk density of the material, the first resonance frequency, and the characteristic impedance of air. This is true only if the normal sound absorption coefficient shows the first resonant peak absorption in the measured frequency range.

Equation (12) is presented in order to show that the amplitude of the resonant absorption does not depend on the thickness of the sample. Consequently, changing the thickness will shift the peak absorptions only in frequencies and not in amplitude.

As the absorption coefficient given by Eq. (11) is valid for low damping loss factors, Fig. 2 shows how this approximation diverges from the exact solution in function of the loss factor. One can note that the absolute error is less than 2% for damping loss factors smaller than 1. Consequently, Eq. (11) can be used with confidence for a large number of elastic closed-cell foams as most of them have a loss factor less than 1.

4. Optimal and reduced damping loss factors

Figure 3 shows how the sound absorption coefficient at first resonance varies with the damping loss factor. The sound absorption coefficient reaches almost 100% absorption for an optimal damping loss factor. This optimal loss factor is deduced from Eq. (11) by setting $\alpha(\omega_1)=1$. This yields:

$$\eta_{opt} = \frac{2Z_0}{\omega_1 \rho_1 L}. \tag{13}$$

Now, one can define the reduced damping loss factor as the ratio of the actual damping loss factor to the optimal value

$$\eta_r = \frac{\eta}{\eta_{opt}}. \tag{14}$$

Substituting Eq. (14) into Eq. (11), the sound absorption at first resonance reduces to

$$\alpha(\omega_1) = 1 - \left| \frac{\eta_r - 1}{\eta_r + 1} \right|^2. \tag{15}$$

Apart from the optimal damping loss factor, Eq. (15) and Fig. 3 show that there exist two reduced damping loss factors for a given value of $\alpha(\omega_1)$. The first solution corresponds to a low damping solution, and the second one corresponds to a high damping solution. These solutions are, respectively,

$$\eta_r^{sol1} = \frac{4 - 2\alpha(\omega_1) - 4\sqrt{1 - \alpha(\omega_1)}}{2\alpha(\omega_1)},$$

$$\eta_r^{sol2} = \frac{4 - 2\alpha(\omega_1) + 4\sqrt{1 - \alpha(\omega_1)}}{2\alpha(\omega_1)}, \tag{16}$$

with $\eta_r^{sol1} \leq \eta_{opt} \leq \eta_r^{sol2}$.

Figure 4 shows the normal incidence sound absorption coefficient of an equivalent solid for the optimal damping loss (13), and the damping loss solutions obtained from Eqs. (14) and (16) with $\alpha(\omega_1)=0.7$. The absorption coefficient is computed using Eqs. (5) and (7) with $L=30$ mm, $\rho_1 = 90$ kg m^{-3}, $K_b = 536$ kPa, and $Z_0 = 412$ Pa s m^{-1}. As expected, the main difference between sol1 and sol2 lies in the width of the peak and not in its amplitude.

Here, the optimal damping introduced through Eq. (13) must be used with caution since it is only valid for a sliding edge condition on small samples, or for samples of laterally infinite extent (or large extent using a free field measuring method[13]). If other boundary conditions are used on small samples, another set of equations needs to be developed.
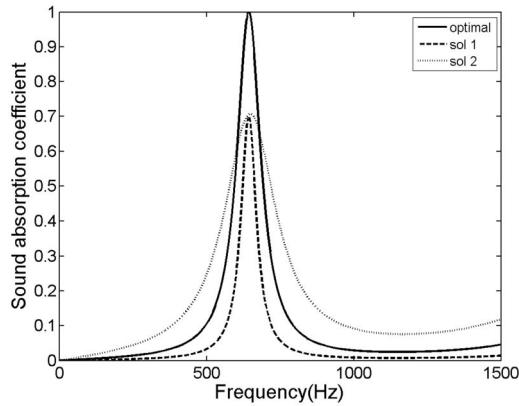
FIG. 4. High and low solutions of the reduced damping loss factor.

FIG. 5. Computation of the bonded correction factor c_b.

B. Bonded edge condition

The previous section has shown the theory of a method to find the bulk Young's modulus and damping loss factor for a sliding sample of solid or closed-cell porous materials on hard backing. Unfortunately, the sliding condition in an impedance tube cannot be perfectly ensured in practice. Therefore, this section extends the proposed method to another type of boundary condition: the bonded edge condition. In this case, the same assumptions as previously defined can be first made (i.e., the Poisson's ratio is assumed to be known and the sound absorption at the resonance is only governed by the bulk damping loss factor).

1. Finding Young's modulus

Considering a bonded edge condition and a hard backing, the first compression resonance depends on the shape factor s and the Poisson's ratio ν. This frequency can be expressed by

$$f_1^b = \frac{\omega_1^b}{2\pi} = \frac{c_b(\nu,s)}{4L}\sqrt{\frac{K_b}{\rho_1}}, \tag{17}$$

where the shape factor s is the ratio of the diameter of the sample to its thickness: i.e., $s = D/L$.

Comparing to the first resonance frequency of a sliding sample given by Eq. (1), Eq. (17) becomes:

$$f_1^b = c_b(\nu,s)f_1. \tag{18}$$

The factor c_b is called the bonded edge correction factor. This coefficient only depends on the shape factor s and Poisson's ratio ν. A two dimensional axisymmetric finite element method (FEM) model has been used in order to compute this coefficient. A CPU Intel Pentium D, 3 GHz, 4 GB RAM has been used for the entire study. An eigenfrequency analysis is employed for the bonded sample. The correction factor c_b is simply the ratio of the first resonance frequency calculated with the FEM model to the frequency given by Eq. (1). Note that the FEM simulations for a sliding sample correlates with Eq. (1). From the FEM results, an abacus of the correction factor is generated—this eliminates the use of FEM simulations in the future. This table contains the bonded correction factor c_b for $s \in [0.05 \ 5]$ and $\nu \in [0 \ 0.499]$. Then, a function is implemented for interpolating the bonded correction factor
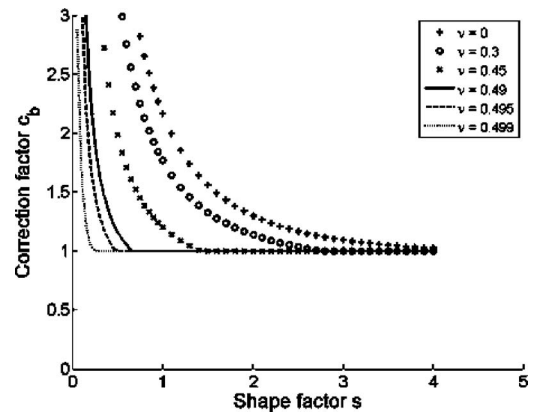
from a given couple (s, ν). Figure 5 shows how this correction factor evolves with the shape factor for some Poisson's coefficients. The low limit of the correction factor is one. A factor below 1 would imply that the first resonance is no longer a compression resonance. The theory would not be valid anymore. Consequently, with a shape factor of 1.5, the method would work for characterizing materials with Poisson's ratio up to 0.45. This is quite acceptable for typical closed-cell foams.

Still assuming that the Poisson's ratio is known, the bulk modulus is obtained from Eqs. (2) and (18), knowing the bulk density ρ_1, the thickness L and the shape factor s of the sample:

$$K_b = \rho_1 \left(4 \frac{f_1^b}{c_b(\nu,s)} L\right)^2. \tag{19}$$

Finally, the Young's modulus is deduced from Eq. (4).

Contrary to the sliding edge condition, when the bonded edge condition is considered, the bonded sample undergoes shear stresses and the Poisson's ratio plays an important role. Taking advantage of this observation, a method for finding the Poisson's ratio from impedance tube absorption tests is given in a next paragraph.

2. Finding bulk damping loss factor

Considering a bonded sample on a hard backing, the sound absorption coefficient at the resonance still reaches a maximum for an optimal damping loss factor η_{opt}^b. This behavior is similar to the sliding case illustrated in Fig. 3. Thus, the sound absorption coefficient could still be expressed by

$$\alpha(\omega_1) = 1 - \left|\frac{\eta_r - 1}{\eta_r + 1}\right|^2, \quad \eta_r = \frac{\eta}{\eta_{\text{opt}}^b}. \tag{20}$$

Once the reduced damping loss factor has been found from the sound absorption at the resonance, the optimal damping loss factor is required. Unfortunately, Eq. (13) cannot be used anymore. Indeed $\eta_{\text{opt}}^b \neq \eta_{\text{opt}}$ and the greatest difficulty lies in obtaining this optimal factor. One calls this factor the bonded edge optimal loss factor in opposition to the sliding edge optimal loss factor defined by Eq. (13). Now, one needs to describe how η_{opt}^b evolves in function η_{opt}. To do so, the bonded edge optimal loss factor is com-

TABLE I. Properties used for the linear relation between the two optimal loss factors

s	ν	c_b	b	ms	K_b (Pa)	η_{opt}^b
3.35	0.2	1.0077	0.083	0.0977	4,038,500	0.095
					448,720	0.105
					200,000	0.12
					134,620	0.13
3.95	0.1	1.008	0.054	0.1075	4,038,500	0.065
					448,720	0.08
					200,000	0.095
					134,620	0.105
1.25	0.3	1.4997	0.001	0.2181	4,038,500	0.015
					448,720	0.04
					200,000	0.055
					134,620	0.07
1.4	0.2	1.5103	0.001	0.2196	4,038,500	0.015
					448,720	0.04
					200,000	0.055
					134,620	0.07
0.5	0.3	3.2744	0.003	0.2535	4,038,500	0.01
					448,720	0.02
					200,000	0.035
					134,620	0.04
0.6	0.1	3.3316	0.000	0.3123	4,038,500	0.01
					448,720	0.025
					200,000	0.035
					134,620	0.045

puted for a number of couples (s, ν). The bulk density of the sample is fixed to 90 kg m^{-3}, its diameter to 30 mm, and the characteristic impedance of the air is fixed to 412 Pa s m^{-1}. The couples (s, ν), the bulk modulus K_b and the bonded edge correction factor c_b are given in Table I. Figure 6 shows the linear relation linking the two optimal loss factors for 3 correction factors c_b. The three graphics correspond to the three sections of Table I, respectively. Each correction factor is obtained from two different couples (s, ν) and a section corresponds to an approximately equivalent correction factor (e.g., 1.0, 1.5, or 3.3). All these cases lead to a linear relation of the form:

$$\eta_{opt}^b = \frac{\pi s}{c_b} m(c_b) \eta_{opt} + b(c_b), \tag{21}$$

where m and b are two factors depending on the bonded edge correction factor c_b.

These factors are computed for a range of correction factors $c_b \in [0,5]$. Figure 7 represents ms and b as functions of the correction factor. For each coefficient, a polynomial approximation is carried out. These polynomial approximations enable a significant simplification for computing the bonded optimal loss factor from the sliding optimal loss factor given by Eq. (13). These polynomial relations are also plotted in Fig. 7 and are expressed as follows:

$$c_b < 2 \Rightarrow m(c_b)s = 0.0028x^5 - 0.0484x^4 + 0.3206x^3$$
$$- 1.0238x^2 + 1.6004x - 0.7462,$$
$$\tag{22}$$
$$c_b \geqslant 2 \Rightarrow m(c_b)s = 0.0256x + 0.1876,$$

and
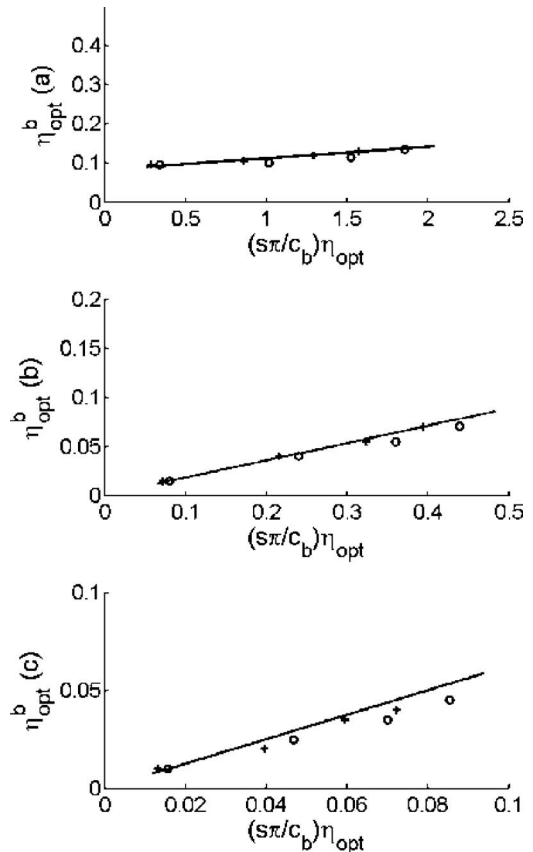
FIG. 6. Linear relation between the bonded and the sliding optimal damping loss factors. (1) c_b=1.0, (2) c_b=1.5, and (3) c_b=3.3.
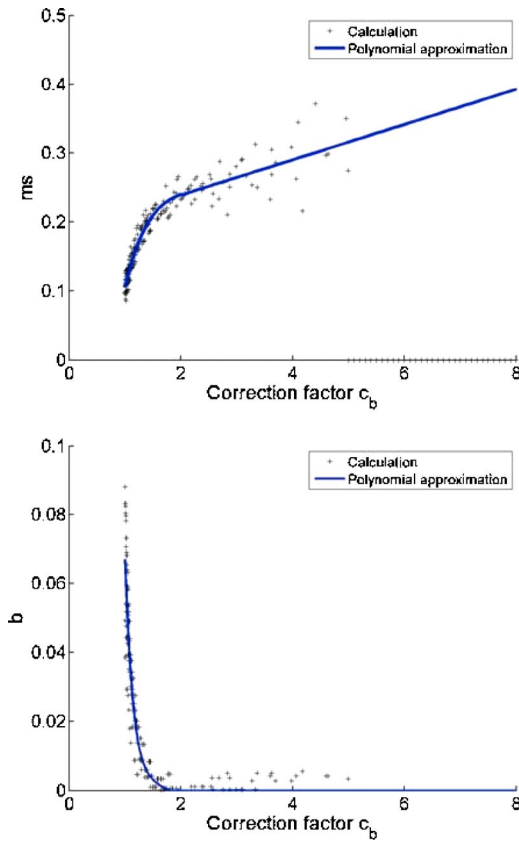
FIG. 7. (Color online) Computations of m and b in function of the bonded correction factor c_b.

$$c_b < 2 \Rightarrow b(c_b) = 0.179x^6 - 2.0054x^5 + 9.2993x^4$$
$$- 22.859x^3 + 31.447x^2$$
$$- 22.996x + 7.0021,$$
$$c_b \geq 2 \Rightarrow b(c_b) = 0. \tag{23}$$

Finally, assuming that the Poisson's ratio is known, the bonded edge correction factor c_b is deduced from the abacus previously computed (see Fig. 5). The coefficients m and b are calculated with relations (22) and (23). Then, the bonded edge optimal loss factor η_{opt}^b is deduced from Eq. (21). The actual damping loss factor is, at last, calculated from the sound absorption coefficient at the resonance using Eqs. (16) and (20).

3. Finding Poisson's ratio

By looking at Eq. (1), one can note that the product $f_1 L$ is kept for the same material. Thus, considering two samples defined by $[\rho_1, K_b, s_1, L_1, f_1^b(\nu, s_1)]$ and $[\rho_1, K_b, s_2, L_2, f_2^b(\nu, s_2)]$, residue R is defined as follows:

$$R = \left| \frac{f_1^b(\nu, s_1)}{c_b(\nu, s_1)} L_1 - \frac{f_1^b(\nu, s_2)}{c_b(\nu, s_2)} L_2 \right|. \tag{24}$$

This residue is equal to zero for an admissible solution of the Poisson's ratio. Due to the nature of c_b, R is similar to a second order polynomial having two roots. Sometimes, two solutions are admissible for the Poisson's ratio. To get
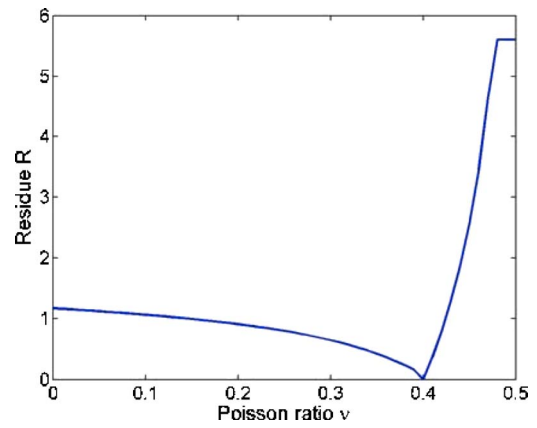

FIG. 8. (Color online) Residue in function of the Poisson's ratio.

around this problem, a third sample is used. This sample is defined by $[\rho_1, K_b, s_3, L_3, f_3^b(\nu, s_3)]$. The residue R becomes

$$R = \left| \frac{f_1^b(\nu, s_1)}{c_b(\nu, s_1)} L_1 - \frac{f_1^b(\nu, s_2)}{c_b(\nu, s_2)} L_2 \right| + \left| \frac{f_1^b(\nu, s_1)}{c_b(\nu, s_1)} L_1 \right.$$
$$\left. - \frac{f_1^b(\nu, s_3)}{c_b(\nu, s_3)} L_3 \right|. \tag{25}$$

Independently of the Young's modulus, the residue is equal to zero for the actual value of the Poisson's ratio. Thus, knowing the three frequencies f_1^b, f_2^b, and f_3^b and the geometries of the samples $(L_1, s_1, L_2, s_2, L_3, s_3)$, the Poisson's ratio can be deduced from the computation of residue R. This computation is illustrated in Fig. 8.

III. EXPERIMENTAL RESULTS

In this section, the previous theory is experimentally tested on two expanding closed foams: one with a sliding edge condition and one with a bonded edge condition. The normal sound absorption coefficients are measured with a 29-mm Bruel & Kjaer 4206 impedance tube following standard ASTM E1050-98 or ISO 10534-2:1998.

A. Sliding edge condition

In this first test, the sample is cut using pressurized water jet to ensure nice circularity and a diameter of $29.0_{-0.2}^{+0.0}$ mm. With this diameter, once mounted in the 29-mm impedance tube, it is assumed the sample can slide freely along the tube axis, and leakage around the sample is negligible. In this case, the first compression resonance frequency and related maximum absorption are easily determined from the measured absorption shown in Fig. 9. These results together with the known material properties and dimensions are listed in Table II

Assuming that the Poisson's ratio is equal to 0.33, the bulk modulus is deduced from Eq. (2) and the Young's modulus using Eq. (4). This yields, respectively, $K_b = 546\,362$ Pa and $E = 368\,753$ Pa. On the other hand, the optimal damping loss factor, reduced damping loss factor, and bulk damping loss factor are obtained from Eqs. (13), (16), and (14), respectively. This yields, $\eta_{\text{opt}} = 0.041$, $\eta_r^{\text{sol2}} = 11.160$, and $\eta = 0.458$.

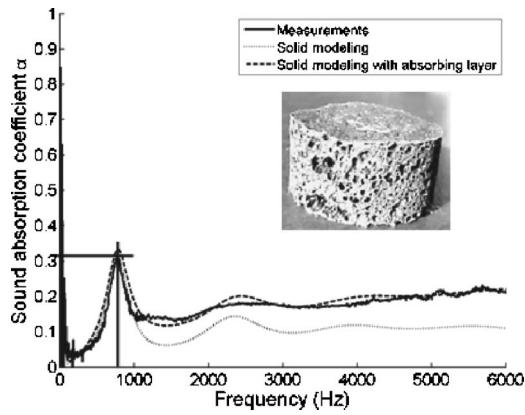F. Chevillotte and R. Panneton: Elastic characterization of foams

FIG. 9. Normal sound absorption coefficient of the tested expanding closed-cell foam with the sliding edge mounting condition. Comparison between impedance tube measurement, solid simulation, and solid simulation with surface absorption.

Using the found parameters, the sound absorption coefficient predicted using the equivalent solid model [Eqs. (5) and (7)] is compared to impedance tube measurements in Fig. 9. The simulation correlates well with the measurement at the resonance peak. However, for frequencies higher than 1000 Hz, the predicted absorption is underestimated. This is due to the fact that the surface sound absorption is not considered with the equivalent solid model (i.e., surface is assumed impervious). In order to correct for this, the solid model with surface absorption proposed in Ref. 4 can be used. In this case, one needs to define the thickness of the surface absorption layer by

$$d = \frac{1}{2} \sqrt{\frac{2P_0}{\omega_{\min} \sigma \phi}}, \tag{26}$$

where $\omega_{\min}$ is a low frequency (here 628 rad s^{-1}, 100 Hz, is used), P_0 the atmospheric pressure (101 325 Pa), and $\sigma \phi$ the product of the static airflow resistivity and open porosity of the surface absorption layer. In this case, the value of $\sigma \phi$ was iteratively found to be $\sigma \phi = 10^7$ N s/m^4. This yields, from Eq. (26), $d = 2.8$ mm, i.e., the thickness of the surface absorption layer (thin resistive layer accounting for the fact the surface is not purely impervious).

Consequently, with a 2.8-mm surface absorption layer covering an 11.3-mm equivalent solid core (total thickness is 14.1 mm), the prediction of the surface absorption model is compared to measurements in Fig. 9. This time the correlation with measurements is excellent for the whole frequency range.

For this material, one can note that the sound absorption at the first resonance is relatively low. This is logical since the actual damping loss factor of the material (0.458) is very far from the optimal value (0.041).

TABLE II. Properties of the 29-mm diameter sample of expanding closed-cell foam used for the sliding Edge Condition test.

Bulk density ρ_1 (kg m^{-3})	299
Thickness L (mm)	14.1
Resonance frequency f_1 (Hz)	776
Sound absorption $\alpha(\omega_1)$	0.308

TABLE III. Properties of the three 29-mm diameter samples of the expanding closed-cell foam used for the bonded edge condition test.

	Sample 1	Sample 2	Sample 3
Bulk density ρ_1 (kg m^{-3})	83.0	80.4	81.8
Thickness L (mm)	18.8	27.1	35.8
Shape factor s	1.60	1.11	0.84
Resonance frequency f_1 (Hz)	1176	992	896
Sound absorption $\alpha(\omega_1)$	0.56875	0.53925	0.51417

B. Bonded edge condition

For this second test, the method is now experimentally tested on samples with the bonded edge mounting condition. Three samples of a different length are required for computing the Poisson's ratio. Here, each foam sample was carefully and directly heat expanded in a hollow cylinder having a 29-mm inner diameter. The part of the foam running over the ends of the cylinder was cut. Then, the cylinder was mounted on the tube using a special end termination ensuring a rigid backing.

The data related to each sample are summarized in Table III, and the absorption curves are given in Fig. 10. Using these data, the Poisson's ratio is calculated with the residue R defined by Eq. (25). This yields $\nu = 0.43 \pm 0.005$.

The correction factor can now be read from the abacus in Fig. 5 and the bulk modulus can be computed for each sample from Eq. (19). In order to obtain a good approximation of the Poisson's ratio, the three shape factors must be different. Moreover, from this abacus, one can note that the correction factors converge to 1 when either the shape factor is increased or the Poisson's ratio is increased. It is thus easier to find low Poisson's ratio ($\nu < 0.45$). The ability to find the Poisson's ratio is increased as the shape factors are decreased.

The Young's modulus can now be deduced from the found Poisson's ratio and the average bulk modulus using Eq. (4). This yields $E = 214\,897 \pm 2853$ Pa. Finally, the optimal damping loss factor is obtained from Eqs. (21) and (13). Similarly to the sliding condition, the actual bulk damping loss factor is deduced from Eqs. (16) and (20). This yields $\eta = 0.22 \pm 0.04$.

The sound absorption coefficient is now computed with the equivalent solid model and compared to the impedance tube measurements in Fig. 10. The correlation with measurements is good especially at the resonance peak. Again, the surface absorption model [4] is used in order to correct for the underestimation of the predicted absorption (here, $\sigma \phi = 5 \times 10^6$ N s/m^4 and $d = 4.01$ mm were used). The residual variation between these latter predictions and the measurements may be attributed to the fact that the real elastic parameters of the expanded foam are not necessarily constant with the frequency.

IV. CONCLUSION

In this work, a method was proposed to determine the bulk elastic properties of soft equivalent solids or closed-cell foams from simple impedance tube absorption tests. The method was tested experimentally with success in laboratory.
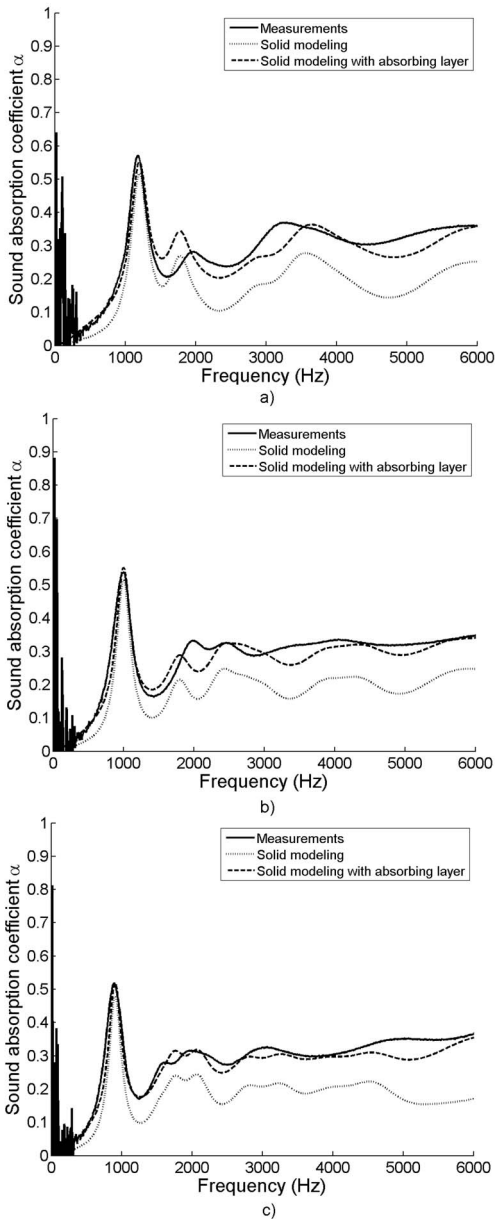
FIG. 10. Normal sound absorption coefficients of the three samples of the tested expanding closed-cell foam with the bonded edge mounting condition. Comparison between impedance tube measurement, solid simulations, and solid simulation with surface absorption. (a) Sample 1; (b) Sample 2; and (c) Sample 3.

It has revealed that the properties found with the proposed method can be used in the surface absorption solid model worked out in Ref. 4 to yield excellent correlations with measurements.

However, the accuracy of the method relies mostly in the proper control of the mounting conditions in the impedance tube. This is actually the most important limitation of the method, especially on small sample diameters for which the absorption measurement is very sensitive to boundary conditions. Further tests are required to validate the robustness of the proposed method.

ACKNOWLEDGMENTS

[1] M. Biot, "The theory of propagation waves in a fluid-saturated porous solid. I. Low frequency range. II. Higher frequency range," J. Acoust. Soc. Am. **28**, 168–191 (1956).

[2] J. F. Allard, *Propagation of Sound in Porous Media. Modeling Sound Absorbing Materials* (Elsevier Applied Science, New York, 1993).

[3] U. Ingard, *Notes on Sound Absorption Technologies* (Noise Control Fundation, New York, 1994).

[4] J.-L. Wojtowicki and R. Panneton, "Improving the efficiency of sealing parts for hollow body network," SAE Tech. Paper, Document No. 2005-01-2279 (2005).

[5] C. Langlois, R. Panneton, and N. Atalla, "Polynomial relations for quasi-static mechanical characterization of poroelastic materials," J. Acoust. Soc. Am. **110**, 3032–3040 (2001).

[6] M. Melon, E. Mariez, C. Ayrault, and S. Sahraoui, "Acoustical and mechanical characterization of anisotropic open-cell foams," J. Acoust. Soc. Am. **104**, 2622–2627 (1998).

[7] Y. K. Kim and H. B. Kingsbury, "Dynamic characterization of poroelastic materials," Exp. Mech. **19**, 252–258 (1979).

[8] A. Wijesinghe and H. B. Kingsbury, "Complex modulus of a poroelastic column," J. Acoust. Soc. Am. **65**, 90–95 (1979).

[9] T. Pritz, "Transfer function method for investigating the complex modulus of acoustic materials: rod-like specimen," J. Sound Vib. **81**, 359–376 (1982).

[10] S. Sim and K.-J. Kim, "A method to determine the complex modulus and Poisson's ratio of viscoelastic materials from FEM applications," J. Sound Vib. **141**, 71–82 (1990).

[11] R. D. Blevins, *Formulas for Natural Frequency and Mode Shape* (Krieger Publishing Co., Malabar, FL,2001).

[12] L. J. Gibson and M. F. Ashby, *Cellular Solids: Structure and Properties*, 2nd ed. (Cambridge University Press, Cambridge, 1997).

[13] J.-F. Allard and P. Delage, "Free field measurements of absorption coefficients on square panels of absorbing materials," J. Sound Vib. **101**, 161–170 (1985).